ILASS-Americas 22nd Annual Conference on Liquid Atomization and Spray Systems, Cincinnati, OH, May 2010

Reduced Order Modeling of Steady and Unsteady Flow over a Sphere

B. T. Helenbrook* and D. R. Witman
Department of Mechanical and Aeronautical Engineering
Clarkson University, Potsdam, NY 13699-5725

Abstract

In this paper, we use the proper orthogonal decomposition (POD) to study forced oscillatory flow over a particle at a range of Reynolds numbers, Strouhal numbers, and velocity oscillation amplitudes relative to the mean flow. A reduced-order model of the response is created by performing a streamwise-upwind-Petrov-Galerkin (SUPG) projection of the incompressible Navier-Stokes equations onto the space spanned by the POD modes generated from the detailed simulations. Several different numerical implementations of the POD are tested to try to reduce the effect of round-off error in the modeling process. Results for steady flows indicate that the drag can be predicted to within 1% of the direct numerical simulations using only 10 modes. For unsteady flows, roughly 40 modes are needed to predict the unsteady response over a Reynolds number range from 0.1 to 100 and a Strouhal number range of 0.1 to 10.

*Corresponding Author: helenbrk@clarkson.edu

Introduction

The study of drops and particles is of importance to many natural and industrial processes such as raindrops and hailstones, atmospheric particle transport, particle transport by rivers and streams, sprays, and aerosols. To simulate these problems, one often uses simplified drag models to predict the coupling between the carrier phase and the discrete particle phase. Simplified models have been developed through analytic, experimental, and numerical studies of individual drops and particles. One such model is the Basset-Boussinesq-Oseen (BBO) equation [1–3] (BBO equation). The BBO equation includes many terms that govern the motion of the particle. These include: forces due to pressure gradients, an "apparent mass" term, a drag force, a lift force, a Basset time history term, and gravitational effects. This model was derived analytically for low Reynolds numbers. At higher Reynolds numbers, the problem is non-linear and it is more difficult to obtain analytic solutions, thus there is no analytic model for the physical effects included in the BBO equation. There are empirical laws available for predicting the steady drag of a sphere [4], but it is more difficult to accurately model more complex effects. On the other hand, detailed numerical studies can be performed [5], [6] at finite Reynolds numbers to find the forces related to the particle evolution equation. However, it is difficult to use this information to create a reliable model for predicting particle evolution.

In our previous work [7], we used "reduced order modeling" techniques [8–10] to develop models for flow over a spherical particle. Specifically, we applied the Proper Orthogonal Decomposition (POD) [8] to detailed numerical simulation data to generate a basis of spatial functions (called "POD modes" or "empirical eigenfunctions") that could compactly represent steady solutions for flow over a sphere at various Reynolds numbers. These modes were then combined with a weighted integral form of the Navier-Stokes equations to generate a predictive model for the flow. Using only 10 POD modes, we demonstrated that the variation of drag as a function of Reynolds can be predicted with less than 1% error.

In this work, we present several improvements on the technique proposed in [7], and we apply the new techniques to forced oscillatory flow over a sphere. The paper begins with an overview of the formulation presented in [7] and then presents several new techniques for generating POD modes that are designed to reduced the impact of numerical round-off errors and eliminate non-physical negative eigenvalues. The benefit of these techniques is then examined for the problem of predicting steady flow over a sphere as a function of Reynolds number. The best performing approach for the steady flow predictions is then applied to create a model of forced oscillatory flow over a sphere as a function of Strouhal number, Reynolds number, and the amplitude of the forcing relative to the free-stream velocity.

Problem Formulation

In this section, we describe the physical problem to which we apply reduced-order modeling techniques. The problem is that of steady and unsteady, axisymmetric fluid flow over a spherical particle. The fluid is assumed incompressible with constant density, ρ, and viscosity, μ. The equations governing the motion of the fluid are the continuity equation and the Navier-Stokes equations. For the unsteady calculations, the free-stream velocity is given by the following function

$$v_\infty = \bar{v}_\infty + Asin(\omega t)$$

where $\bar{v}_\infty$ is the mean flow velocity, A is the amplitude variation and ω is the angular frequency of the oscillation. The non-dimensional parameters of the problem are the the amplitude ratio, $A/\bar{v}_\infty$, the Strouhal number, $St = \omega d/\bar{v}_\infty$, and the Reynolds number, $\rho\bar{v}_\infty d/\mu$ where d is the sphere diameter.

The numerical formulation of the above problem follows the work presented in [11]. We write the governing equations in terms of curvilinear coordinates

$$r = r(\xi, \eta), z = z(\xi, \eta) \tag{1}$$

where r and z corresponds to our two-dimensional Cartesian coordinate system (since we are dealing with axisymmetric flow they are the radial and axial directions respectively) and ξ, η are independent curvilinear coordinates. Using this notation the incompressible Navier-Stokes equations in curvilinear coordinates can be expressed as

$$diag[0, 1, 1]\frac{\partial \vec{w}}{\partial t} + \frac{\partial \vec{e}}{\partial \xi} + \frac{\partial \vec{f}}{\partial \eta} - \vec{\theta} = 0 \tag{2}$$

where $\vec{w}$ is the vector of unknowns given by $(p, \rho u, \rho v)$ where p is the pressure and u and v are the radial and axial velocity components. $\vec{e}$ and $\vec{f}$ are the total flux vectors of mass and momentum in the ξ and η directions and $\vec{\theta}$ is a source term required because the flow is axisymmetric.

An *hp*-finite element method is used to perform the detailed numerical simulations [11]. The discrete form of Eq. 2 is written using a streamwise-upwind-Petrov-Galerkin (SUPG) variational approach [12].

This allows us to seek solutions for the velocity and the pressure in the same polynomial space [13, 14] without pressure decoupling problems. The form of the equations is as follows

$$0 = \sum_{e=1}^{n_{el}} \left\{ \int\int_{\Omega} \left[\vec{\phi}^T \left(diag[0,1,1] \frac{\partial \vec{w}}{\partial t} - \vec{\theta} \right) \right.\right.$$

$$\left. - \frac{\partial \vec{\phi}^T}{\partial \xi} \vec{\mathrm{e}} - \frac{\partial \vec{\phi}^T}{\partial \eta} \vec{\mathrm{f}} \right] d\Omega + \int_{\Gamma} \vec{\phi}^T \left(\vec{\mathrm{e}}, \vec{\mathrm{f}} \right) \cdot \vec{\mathrm{n}}_{\Gamma} d\Gamma$$

$$+ \int\int_{\Omega} \left[\frac{\partial \vec{\phi}^T}{\partial \xi} \mathrm{A}_{\xi} + \frac{\partial \vec{\phi}^T}{\partial \eta} \mathrm{A}_{\eta} \right]$$

$$\left. \mathrm{T} \left[\left(diag[0,1,1] \frac{\partial \vec{w}}{\partial t} - \vec{\theta} \right) + \frac{\partial}{\partial \xi} \vec{\mathrm{e}} + \frac{\partial}{\partial \eta} \vec{\mathrm{f}} \right] d\Omega \right\}$$

$$\forall \vec{\phi} \tag{3}$$

where the sum is performed over all of the elements in the mesh, 1 to n_{el}. The solution for (p, u, v) is sought in the space $[\Phi]^3$ where Φ is a globally continous finite element space. Each integral in the sum is performed over either the standard triangle area Ω or the standard triangle perimeter Γ. The matrices A_ξ, A_η and T are associated with the SUPG stabilization. For more information on these matrices see [11]. If the term involving T is removed, we recover the standard Galerkin formulation.

For the calculations presented in this study we use a basis composed of quartic polynomials on each element ($P = 4$). Quartic polynomials are used because they allow rapid convergence to the exact drag value with increasing mesh resolution (5th order spatial accuracy). An unstructured triangular mesh on a rectangular domain is used in all the calculations. Figure 1 shows the element mesh used to calculate the detailed solutions for the POD study of flow over a sphere. For the calculations, an inflow condition is enforced at the lower boundary of the mesh with $(u, v) = (0, v_\infty)$ such that the flow is from bottom to top. At the downstream and right boundary, the total stress is set to zero. Along the centerline, a symmetry boundary condition is imposed, and on the sphere, which is centered at (0,0), a no slip boundary condition is imposed. The downstream boundary is from (0, 30) to (20, 30), and the inflow boundary is from (0, -20) to (20, -20) where the units are sphere diameters. It is shown in [7] that we are able to obtain values of drag with at least 1% accuracy using this configuration.

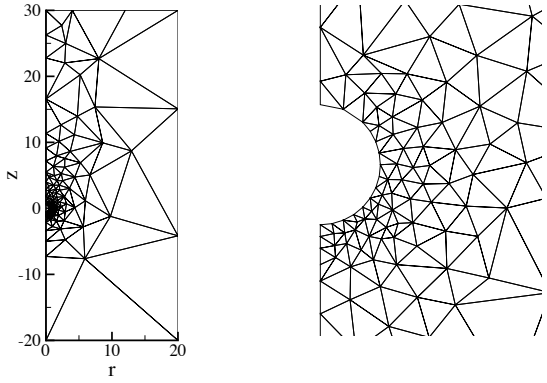

Figure 1. Typical element mesh and magnified region around the sphere

POD Based Modeling

The POD was introduced by Lumley [8] as a means to extract the large scale structure of turbulent flows. It uses data obtained in experiments or numerical simulations to generate an orthogonal set of spatial basis functions that optimally describe the flow's energy. The POD finds functions (herein called POD modes) that maximize the mean square inner product of the flow solutions with the POD mode, $\vec{\varphi}$

$$\frac{\langle \left(\int_{\Omega} \vec{u} \cdot \vec{\varphi} d\Omega \right)^2 \rangle}{\int_{\Omega} \vec{\varphi} \cdot \vec{\varphi} d\Omega} \tag{4}$$

where $\vec{u}$ is the spatial flow field (u, v), Ω is the physical domain, and the angled brackets $\langle\rangle$ indicate an averaging process. The average is taken over all of the solutions obtained. If these solutions are unsteady, then the averaging is a temporal average. This is not necessarily the case however. The average could include steady solutions obtained at different Reynolds numbers. In the following, we will use the averaging in a general sense, and t can indicate either different Reynolds number solutions or unsteady solutions. The POD mode is optimal because it will represent all of these solution as well as possible in the mean square sense.

Solutions to the above maximization are obtained by solving the Fredholm equation

$$\int_{\vec{x}'} \mathbf{R}(\vec{x}, \vec{x}') \vec{\varphi}(\vec{x}') d\vec{x}' = \lambda \vec{\varphi}(\vec{x}), \tag{5}$$

where $\mathbf{R}(\vec{x}, \vec{x}')$ is an autocorrelation tensor

$$\mathbf{R}(\vec{x}, \vec{x}') = \langle \vec{u}(\vec{x}, t) \vec{u}(\vec{x}', t)^T \rangle. \tag{6}$$

Because the autocorrelation function is symmetric, this problem generates an orthogonal series of POD modes similar to an algebraic eigenvalue problem.

The first POD mode satisfies the maximum property given above. The next POD mode is orthogonal to the first, and satisfies a similar maximum property except that it maximizes against the remainder of the flow field that can not be captured using the first mode. The higher modes are similar. In this way, a hierarchy of functions is generated that can represent the transient or parametric flow variations with as few degrees of freedom as possible. The eigenvalues, λ, of the Fredholm equation represent the mean energy captured by each mode, $\vec{\varphi}$.

When applied to data obtained from numerical simulations or experiments, the discrete form of Eq. 5 becomes an N dimensional eigenvalue problem where N is the number of data points. Often numerical and experimental data sets are highly resolved ($N \gg 1$), which makes it difficult to solve this problem. A more efficient method proposed by Sirovich [15] allows us to reduce the size of the eigenvalue problem. The main idea of Sirovich's method is to write the POD modes as a linear combination of "snapshots" of the instantaneous flow field

$$\vec{\varphi} = \sum_{k=1}^{M} \psi_k \vec{u}_k, \tag{7}$$

where the sum is performed over the number of snapshots, M, used in the discrete time average for Eq. 6. By substituting this equation into Eq. 5 we arrive at the following analogous eigenvalue problem

$$C\vec{\psi} = \lambda\vec{\psi}, \tag{8}$$

whose discrete matrix entries are given as

$$C_{kl} = \frac{1}{M} \int_{\vec{x}} \vec{u}(\vec{x}, t_k) \cdot \vec{u}(\vec{x}, t_l) d\vec{x}, \tag{9}$$

This method involves solving an eigenvalue problem that has dimension M. The snapshot method is thus more efficient whenever the number of snapshots, M, is smaller than the number of grid points, N.

Implementation of POD

In this section we give an overview of the numerical procedure used to determine the POD modes. We always use the snapshot method because we typically have fewer snapshots than grid points in the computational mesh. A component (u or v) of the hp-finite element flow solution, $\vec{u}$, in equation 8 can be represented as follows

$$u_i(\vec{x}, t_l) = \sum_{j=1}^{N} c_{i,l,j} \gamma_j(\vec{x}), \tag{10}$$

where $c_{i,l,j}$ is the solution coefficient for flow component i, at time step t_l, for hp-finite element basis function, $\gamma_j(\vec{x})$. If we substitute this expansion into Eq. 9 and integrate over the domain we arrive at the following integration formulation

$$C_{kl} = \frac{1}{M} \int_{\vec{x}} \sum_{i=1}^{2} \sum_{j=1}^{N} c_{i,k,j} \gamma_j(\vec{x}) \sum_{j=1}^{N} c_{i,l,j} \gamma_j(\vec{x}) d\vec{x}, \tag{11}$$

which can be numerically integrated using Gauss integration. Details of the discrete integration formulation can be found in [16]. To help reduce round-off errors, rather than simply accruing the results from each element into a single variable, the results from each element are stored in a vector, s, having a length equal the number of elements in the mesh. This vector is then added pairwise using the following algorithm

```
N = length(s)
while (N > 1)
   for i = 1:N/2
      s(i) += s(N/2+i)
   end
   if (N is odd) s(N/2) += S(N)
   N = N/2
end
```

This algorithm avoids adding numbers of much different magnitude. For example to add a vector of length 1024 with each entry being 1, a standard accrual will result in the final addition of 1 to 1023 which requires four significant digits to be accurate. In the above algorithm, the final addition would be 512+512 which only requires one significant digit to be accurate to within 2.4%. The importance of low-round-off addition versus standard accrual will be shown in the results section.

The eigenvalue problem given by eq. 8 is solved using Lapack's DSPEV routine. As we show in the following, there is typically a large variation in the magnitude of the eigenvalues, and the eigenvalue problem is stiff. This often leads DSPEV to return non-physical negative eigenvalues. As an alternative, we investigate a modified approach for solving eq. 8. The idea is based on the fact that the POD modes are repeated solutions of eq. 4. In the modified approach, we begin by forming 8 using the flow snapshots. DSPEV is then used to find only the largest eigenvalue and eigenvector. This eigenvector is used to form the first POD mode following eq. 7. The next step of the process is then to remove the projection of this mode from each snapshot

$$\vec{u}^{[\nu+1]} = \vec{u}^{[\nu]} - (\vec{u}^{[\nu]} \cdot \vec{\varphi})\vec{\varphi}$$

where the superscript of $\nu+1$ indicates the modified snapshots and ν indicates the original snapshots. Af-

ter this is completed, the entire process is repeated to find the second POD mode and so on.

A final permutation of the algorithm that has been analyzed is to investigate two different definitions of the inner product used throughout the POD derivation. The standard inner product of $\vec{u} \cdot \vec{\varphi}$ is to include only velocity components in the dot product so that $\vec{u} \cdot \vec{u} = u^2 + v^2$. In our POD formulation we include the pressure in the POD decomposition so $\vec{u}$ is defined as (u, v, p) where p is the pressure. The problem with this definition is that the inner product is not dimensionally consistent having the addition of velocity squared with pressure squared. This problem was discussed in detail in [7]. In that work a low Mach number expansion was performed with $\vec{u}$ defined as $(u, v, \sqrt{p/\rho})$. This resulted in a definition of the inner product that only included the velocity components such that $(u, v, p) \cdot (u, v, p)$ is defined as $u^2 + v^2$. In the following, we compare this choice to a definition which non-dimensionalizes p by the free-stream velocity: $(u, v, p) \cdot (u, v, p) = u^2 + v^2 + p^2/(\rho^2 \bar{v}_\infty^2)$.

Once the eigenvalues and eigenvectors of eq. 8 are found we generate a set of POD modes for the velocity and the pressure as

$$\vec{\varphi} = \sum_{k=1}^{M} \psi_k \begin{bmatrix} p_k \\ u_k \\ v_k \end{bmatrix}. \tag{12}$$

where k is the index of the snapshot. These modes are then normalized such that $\int \vec{\varphi}^n \cdot \vec{\varphi}^m d\vec{x} = \delta_{nm}$. The exact flow field for (u, v, p) can now be reconstructed as follows

$$\begin{bmatrix} p(\vec{x}, t_k) \\ u(\vec{x}, t_k) \\ v(\vec{x}, t_k) \end{bmatrix} = \sum_{n=1}^{M} a_n(t_k) \begin{bmatrix} \varphi_p^n(\vec{x}) \\ \varphi_u^n(\vec{x}) \\ \varphi_v^n(\vec{x}) \end{bmatrix}, \tag{13}$$

where a_n is some expansion coefficient associated with each mode. If we want to further reduce the dimensionality of the approximation, we can use only S of our POD modes instead of the full sum up to M where $S < M$.

Low-dimensional Model

To obtain a low-dimensional model of the flow we perform a streamwise-upwind-Petrov-Galerkin projection of the incompressible Navier-Stokes equations onto the space spanned by the POD modes. We use this approach because it yields better results than the standard Galerkin projection. In certain cases, the standard Galerkin projection suffers from decoupling problems.

The solution for (u, v, p) is sought in the space spanned by a subset of our POD modes, $\vec{\varphi}$. By inserting the expansion given in Eq. 13 into the total flux vectors of the SUPG formulation of the Navier-Stokes equation (Eq. 3) and also using the POD modes as the test functions, we obtain S scalar equations for the expansion coefficients a_n. If we define $R(a_n)$ as the residual error of the Navier-Stokes equations evaluated using the current estimate of the solution, our system becomes

$$R(a_n) = 0, \tag{14}$$

which is solved using a Newton-Raphson iterative technique. After we find these coefficients, we are able to reconstruct the flow field (Eq. 13) and calculate the drag. We can perform the same technique for a standard Galerkin projection by setting the stabilization term in the SUPG formulation equal to zero.

Steady Results

In this section, we analyze the ability of the low-dimensional model to predict steady flow over a sphere as a function of Reynolds number. The POD modes are computed from steady solutions at thirty-five Reynolds numbers varying from $Re = 0.1$ to $Re = 100$ in mulitplicative increments of $10^{1/34}$. Figure 2 is a plot of the eigenvalues versus the mode number. Four different curves are shown. The first is the eigenvalues returned from DSPEV. The second is the eigenvalues using the recursive method of finding the modes. The third is the same except using standard accrual instead of low round-off addition. The fourth is using the recursive method with low round-off addition except with the dot product defined to not include any pressure component. For all cases, we can see that the first mode captures most of the energy in the flow, and there is an exponential decay as we increase the mode number. This shows that the series can be truncated with a relatively small number of modes and yet still capture most of the energy of the flow. The first three of the curves should be identical if there were no round-off errors. The use of low round-off addition seems to make very little difference, however for the standard method of finding the eigenvalues, all eigenvalues past 28 are negative which is non-physical.

Figures 3 & 4 show the streamlines of the first two normalized modes. Both figures give a close-up view to better show the structures around the sphere. The first POD mode is essentially the mean of the snapshots. From the streamlines of the second POD mode, we can see that it captures Reynolds number variation of two main features of the solution. The first is the thickness of the boundary layer that occurs near the surface of the sphere. The second is the recirculation zone at the aft end of the

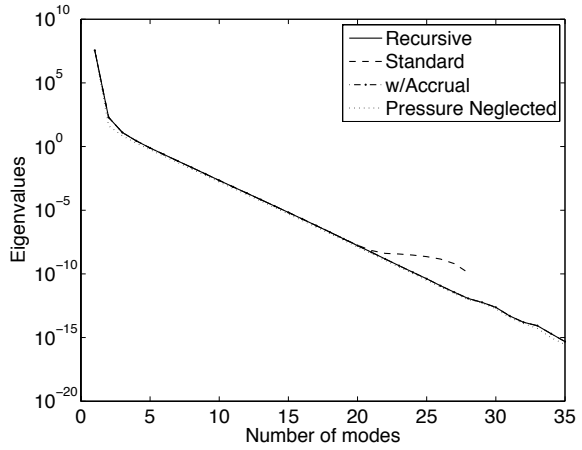

Figure 2. POD Mode Eigenvalues

sphere that is also captured in the first POD mode. Thus, not only are the modes useful for compactly representing the solution, they also give physical insight into the dependence of the flow on Reynolds number.

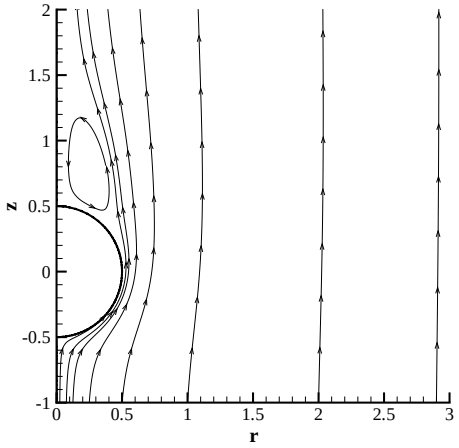

Figure 3. Streamlines of first normalized POD mode

To obtain a reduced-order model of the flow we project the incompressible Navier-Stokes equations onto the space spanned by the POD modes. This enables us to find the expansion coefficients, a_n, that describe the solution at any given Reynolds number. To quantitatively evaluate the POD technique, low-dimensional simulations are performed to determine how many POD modes are needed to accu-

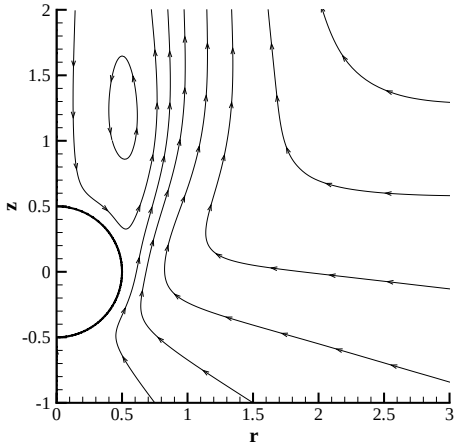

Figure 4. Streamlines of second normalized POD mode

rately predict the drag. Solutions are obtained using $S = 1, 2, 3$, etc... Figure 5 shows the percent error in drag from the detailed simulations versus the number of modes used for various Reynolds numbers. The figure shown is for the recursive method of finding the POD modes including low-round-off addition. As we increase the number of modes, we

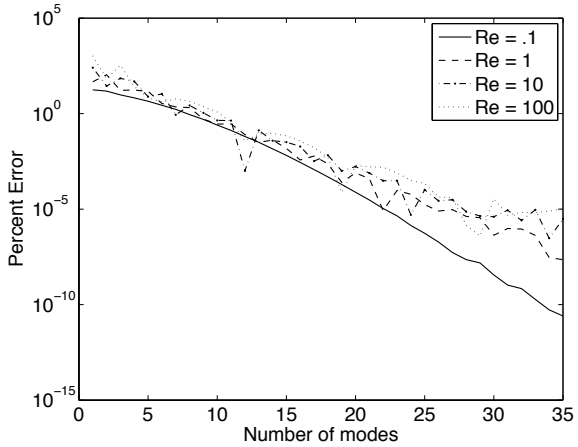

Figure 5. POD Model - Percent Error vs. Number of Modes

see an exponential decrease in the error as shown by the semi-log scale. An 11 mode simulation predicts the drag to within 1.0% over the entire range of Reynolds numbers. Thus, the POD approach can be used to generate compact and accurate models

for particle flows.

Unsteady Results

For the unsteady case, we consider Reynolds numbers of 0.1, 1, 10, and 100 and Strouhal numbers of 0.1, 0.5, 1, 2.0, and 10. For this initial investigation, we keep the amplitude ratio fixed at 0.1. For each case, detailed simulations are run with 15 time steps per period using a 3rd order accurate diagonally implicit Runge-Kutta scheme (DIRK). Each simulation is run for 50 periods to ensure that the simulations reach a periodic state. The last period of time steps are used from each Re and St number combination to generate a set of modes that can span the entire range of conditions. In total, 300 snapshots are used to generate the modes (4 Reynolds numbers by 5 Strouhal numbers by 15 time steps). Figure 6 shows the absolute value of the eigenvalues from the POD decomposition. The dashed curve is calculated using the standard approach, and the solid curve is the recursive approach to finding the eigenvalues. For the standard approach, all eigenvalues beyond 180 are negative.

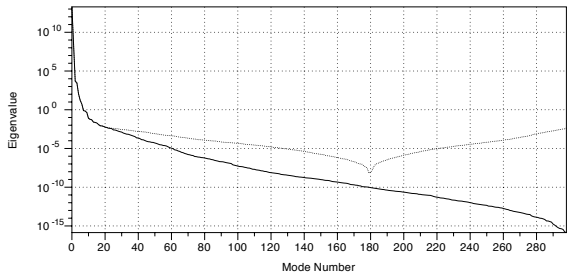

Figure 6. POD mode eigenvalues for unsteady problem

Figure 7 shows the drag response versus time step for four of the Reynolds number / Strouhal number combinations. In the four frames of the figure, the detailed calculations are shown from time step 700 to time step 750. The POD model calculations are restarted from the detailed solutions at time step 735 (one period before the end of the detailed simulation) and continue to time step 795 (4 periods). For the POD model calculations, there are two curves, one was created using a model with 20 modes and the other with 60 modes. It is difficult to tell the two curves apart except at the peaks of the curves where some differences are apparent. For time-steps 735 to 750 the detailed results overlap the POD model results so the model and detailed curves can be directly compared. From this figure, we can see that the reduced order model well predicts the unsteady drag response. With 20 modes, the maximum difference for the cases shown is 4%. For the 60 mode model it is less then 1%. Over the range of Reynolds numbers and Strouhal numbers studied, the maximum difference occurs for the Re=1, St=1 case. In this case, the errors in the peak drag are 10% for the 20 mode model and still less than 1% for the 60 mode model.

We have yet to finish investigating the effect of different POD models on the unsteady results. All of the above were done with the recursive POD mode determination and the low round-off addition using the dot product that includes the scaled pressure. Future work will investigate the effect of the different implementations on the performance of the unsteady model.

Conclusions

We have applied a new modeling technique based on the Proper Orthogonal Decomposition (POD) to unsteady flow over a sphere. This approach allows one to systematically create compact models from detailed solutions. These models can then represent physical phenomena such as unsteady effects that are difficult to model using empirical approaches. Because the models are low-dimensional they can be used in more complex simulations such as spray or particle-laden flow simulations.

Several different implementations were investigated and it was shown that round-off error can significantly impact the performance of the models. A new method of determining the POD modes was found that avoids the non-physical negative eigenvalues that occur when using the standard Lapack-based approach.

Using POD modes obtained from steady solutions of flow over a sphere at Reynolds numbers ranging from 0.1 to 100, a reduced-order model was created to predict the steady drag on a sphere. With only 10 degrees of freedom, this model reproduced the drag response to within 1% of the detailed simulations. For the unsteady simulations, a model was created that included 20 modes and predicted the drag response over two orders of magnitude in Strouhal number and 4 orders of magnitude in Reynolds number. The maximum error in instantaneous drag over this entire range was less than 10% confirming that accurate and compact models can be made of complex phenomena.

References

[1] A. B. Basset. *A Treatise on Hydrodynamics*, volume 2. Cambridge: Deighton, Bell and Co., 1888.

[2] J. Boussinesq. *Theorie Analytique de la Chaleur (L'École Polytechnique, Paris)*, volume 2. 1903.

[3] C. W. Oseen. *Hydrodynamik*. Leipzig: Akademische Verlagsgesellschaft, 1927.

[4] R. Clift, J. R. Grace, and M. E. Weber. *Bubbles, Drops, and Particles*. Academic Press, 1978.

[5] R. Mei, C. J. Lawrence, and R. J. Adrian. *J. Fluid Mech.*, 233:613–631, 1991.

[6] I. Kim, S. Elghobashi, and W. A. Sirignano. *J. Fluid Mech.*, 367:221–253, 1998.

[7] B. J. O'Donnell and B. T. Helenbrook. *Atomization and Sprays*, 15(4):363–376, 2005.

[8] J. L. Lumley. The structure of inhomogeneous turbulent flows. In A.M. Yaglom and V.I. Takarski, editors, *Atmospheric Turbulence and Radio Wave Propagation*, pp. 166–178. Nauka, Moscow, 1967.

[9] B. O. Almroth. *AIAA J.*, 16:525–528, 1978.

[10] D. A. Nagy. *Computers and Structrures*, 10:683–688, 1979.

[11] B. T. Helenbrook. *Comp. Meth. Appl. Mech. Eng.*, 191(3–5):273–294, November 2001.

[12] T. J. R. Hughes and M. Mallet. *Comp. Meth. App. Mech. Eng.*, 58:305–328, 1986.

[13] I. Babuška. *Numer. Math.*, 20:179–192, 1973.

[14] I. Babuška. *Rev. Fr. Autom. Inf. Rech. Oper.*, 8:129–151, 1974.

[15] L. Sirovich. *Quarterly of Applied Mathematics*, 45(3), 1987.

[16] S. J. Sherwin and G. E. Karniadakis. *Comp. Meth. App. Mech. Eng.*, 123:189–229, 1995.

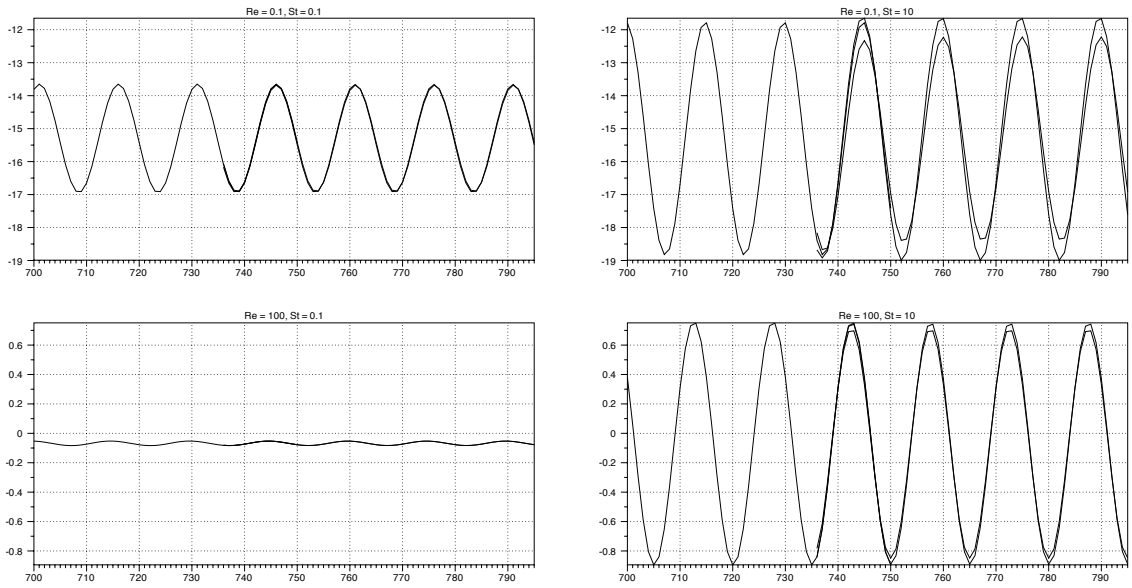

Figure 7. Unsteady response of the detailed simulations and the reduced-order model with 20 and 60 modes. Four conditions are shown: the upper two figures show Re=0.01 with St = 0.1 and 10.0. The lower figures show Re = 100 with St = 0.1 and 10.0